Materials Transactions, Vol. 54, No. 3 (2013) pp. 286 to 290

Microstructure and Mechanical Properties of Cu–Zr–Al Bulk Metallic Glass with Addition of Co

Wei Zhou, Yiming Tao, Li Liu, Lingti Kong, Jinfu Li* and Yaohe Zhou

State Key Laboratory of Metal Matrix Composites, School of Materials Science and Engineering, Shanghai Jiao Tong University, Shanghai 200240, P. R. China

$(Cu_{46}Zr_{46}Al_8)_{100-x}Co_x$ ($x = 0$, 1, 2, 3 and 4) bulk metallic glasses (BMGs) were synthesized by copper mold casting, and the effect of Co addition on the microstructure and mechanical properties of $Cu_{46}Zr_{46}Al_8$ BMG was investigated. The existence of immiscibility gap between Co and the main component Cu is responsible for liquid separation to form droplet-type structure during solidification. The size scale for the droplet-type structure trends to increase with the Co concentration. Depending on the glass-forming ability of the separated liquid phase, amorphous/amorphous or amorphous/crystalline composite structure can be obtained. The results of compression test reveal that the plasticity and the fracture strength can be simultaneously enhanced with an appropriate amount of Co addition owing to nanoscale phase separation with the formation of Cu-rich and Co-rich glassy phases. [doi:10.2320/matertrans.M2012375]

(Received November 12, 2012; Accepted December 17, 2012; Published February 1, 2013)

Keywords: *bulk metallic glass, cobalt addition, phase separation, mechanical properties*

1. Introduction

Different from traditional crystalline materials, bulk metallic glasses (BMGs) lack translational or orientational long-range order. Their plastic deformation at room temperature is generally highly localized into narrow shear bands rather than globally dispersed through the multiplication and slide of dislocations.[1] As a result, failure of BMGs generally occurs along a single shear band without much macroscopic plasticity.[2] The lack of macroscopic plasticity therefore limits their applications as engineering materials. In accord, various approaches have been proposed to remedy such deficiency. Most of them were focused on adding or *in situ* precipitating crystalline phases in the BMG matrix.[3] However, the presence of a second phase generally worsens their glass forming ability,[4] and it may also degrade of some properties, such as yield strength[5] and corrosion resistance.[6] Other methods including enhancing the poisson's ratio[7] and introducing a large amount of free volume[8] have been developed.

Recently, Oh *et al.*[9] reported an excellent plasticity for the Cu–Zr–Al BMG by addition of 7 at% Ag, where phase separation resulted in a composite of Cu-rich and Ag-rich glassy phases. Similar results were also found in the Zr–Cu–Ni–Al[10] and Ti–Zr–Cu–Ni–Sn[11] alloy systems. However, in a recent work, Park *et al.*[12] reported a nanoscale phase separation when adding above 15 at% Y to the Cu–Zr–Al based alloy, forming a composite of Cu-rich and Y-rich glassy phases, which does not exhibit any plastic strain upon deformation. Similar phenomenon was also reported in the $Cu_{40}Zr_{40}Al_{10}Ag_{10}$ BMG.[13] It can be seen that whether the structure of phase separation can enhance the plasticity is still in debate, and the detailed mechanism for the formation of phase separation and its effect on the plasticity of BMG are still far from being understood, and further investigation is needed. Therefore, in the paper, Co was selected as the alloying element, which exhibits a positive heat of mixing with the main constituent Cu in the Cu–Zr–Al alloy, to study its effect on the microstructure and mechanical properties of $Cu_{46}Zr_{46}Al_8$ BMG.

*Corresponding author, E-mail: jfli@sjtu.edu.cn

2. Experimental Procedure

Alloy ingots with nominal compositions of $(Cu_{46}Zr_{46}Al_8)_{100-x}Co_x$ ($x = 0$, 1, 2, 3 and 4) were prepared by arc melting a mixture of pure Cu (99.99%), Zr (99.9%), Al (99.99%) and Co (99.99%) under a Ti-gettered argon atmosphere. The ingots were inverted and remelted six times to ensure chemical homogeneity, and then suction cast into water-cooled copper molds to obtain 50 mm long cylindrical rods with a diameter of 2 mm. Thermal analyses concerning crystallization process were performed using a Pyris Diamond differential scanning calorimetry (DSC) at a constant heating rate of 20 K/min under a flow of high-purity argon. Structure of rod sample was examined using a Thermo ARL X-ray diffractometer (XRD) with monochromatic Cu $K\alpha$ radiation and a JEOL JEM-2100F high-resolution transmission electron microscope (HRTEM). The TEM foils were prepared by electrochemical twin-jet polishing in a solution of 5% perchloric acid and 95% ethanol at 233 K, followed by ion milling with liquid nitrogen cooling. Then the TEM foils were immediately observed under TEM since the thin foils readily oxidize upon exposure to air. Uniaxial compression test was performed on a Sans CMT 5105 testing machine at room temperature under a strain rate of $2 \times 10^{-4}\,s^{-1}$. The test samples were cylinders with a length of 4 mm and a diameter of 2 mm, and the two ends of each sample were polished carefully to ensure parallelism. At least four measurements were conducted for each alloy to obtain reliable results. The fractured samples were examined using a scanning electron microscope (SEM).

3. Results and Discussion

Figure 1 presents the XRD patterns obtained for the $(Cu_{46}Zr_{46}Al_8)_{100-x}Co_x$ rods with a diameter of 2 mm. Each of them has a broad diffuse peak characteristic of the amorphous structure. No evident crystalline peak is found within the

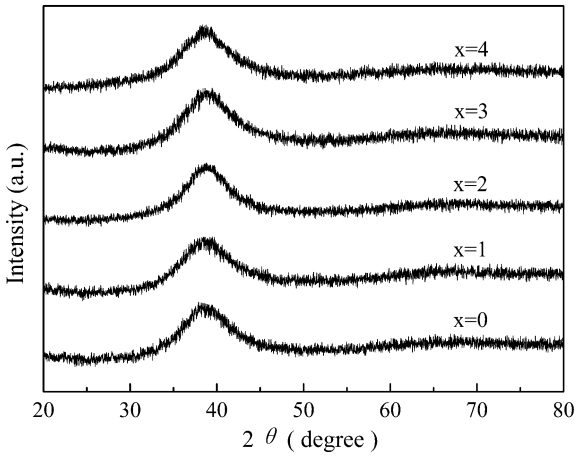

Fig. 1 XRD patterns of the $(Cu_{46}Zr_{46}Al_8)_{100-x}Co_x$ rods with a diameter of 2 mm.

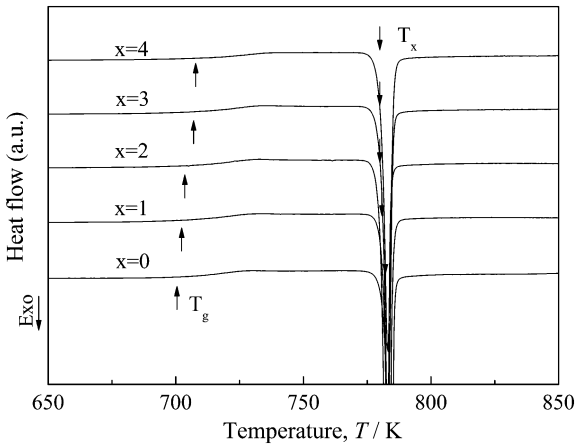

Fig. 2 DSC curves heating at 20 K/min for the $(Cu_{46}Zr_{46}Al_8)_{100-x}Co_x$ alloys.

sensitivity of the XRD employed. Figure 2 shows the DSC traces for the $(Cu_{46}Zr_{46}Al_8)_{100-x}Co_x$ alloys at a heating rate of 20 K/min. Each sample exhibits a clear endothermic event characteristic of glass transition process, and followed by a wide supercooled liquid region and then an exothermic reaction due to crystallization. It seems that the addition of Co does not notably change the crystallization mode. All the crystallizations take place through a single stage. The glass transition temperature T_g increases gradually from 701 to 708 K, while the onset crystallization temperature T_x decreases slightly from 783 to 780 K with increasing Co content from 0 to 4 at%. As a result, the supercooled temperature region width ΔT_x, which reflects the resistance to crystallization of the supercooled liquid, decreases from 82 to 72 K.

HRTEM was used to carefully examine the microstructure of the samples. A homogeneous contrast in the bright-field image and two diffraction haloes in the selected area electron diffraction (SAED) pattern were found for $(Cu_{46}Zr_{46}Al_8)_{100-x}Co_x$ samples with $x = 0$ and 1, as shown in Figs. 3(a) and 3(b), further confirming the formation of glassy phase in the alloys. For the alloy with $x = 2$, however, the TEM image reveals the existence of two distinct phases with different contrasts, as shown in Fig. 3(c). One sees that spherical dark phase with diameter ranging from 5 to 10 nm distributes homogeneously in a bright contrast matrix. The HRTEM image obtained from the local region containing these two contrast phases shows that no lattice fringe was found in either phase or the annular interface areas (Fig. 3(d)). The corresponding SAED pattern does not show any diffraction spots, confirming that these two phases are both fully amorphous. Based on nanobeam EDS analysis with a beam size of 2 nm, the average compositions of the bright and dark glassy phases are $Cu_{47}Zr_{45.1}Al_{6.7}Co_{1.2}$ and $Cu_{43.1}Zr_{45.9}Al_{7.4}Co_{3.6}$, respectively. These results indicate that two glassy phases with different chemical compositions formed by liquid separation during solidification. The bright contrast matrix corresponds to a Cu-rich glassy phase, while the dark contrast droplet is a Co-rich glassy phase. For the alloy with more than 2 at% Co content, the scale of the droplet size increase gradually with increasing Co content. The average sizes of the dark phase for the alloys with $x = 3$ and 4 are 10–15 and 15–20 nm, respectively. Moreover, nanocrystalline phase also appears in the amorphous matrix, and its average size is almost the same with that of the dark phase, as displayed in Figs. 3(e) and 3(f).

As mentioned earlier, large negative heats of mixing among the constituent elements can facilitate the glass formation of an alloy. On the contrary, phase separation may occur if repulsive interactions present among the constituent elements.[14] Based on the present and previous studies,[15] like Cr, addition element Co also exhibits a positive heat of mixing with Cu, phase separation was detected in the Cu–Zr–Al–Co alloy system under HRTEM observation, but not found in the Cu–Zr–Al–Cr alloy system. These results raise an intriguing question that what factors contribute to different microstructures for these two alloys. As we know, the degree of local heterogeneity in the glassy matrix depends strongly on the alloy composition. The difference in the value of mixing heat between the Co–Cu ($\Delta H_{Co-Cu} = +6$ kJ/mol) and Co–Zr ($\Delta H_{Co-Zr} = -41$ kJ/mol) is more considerable than that between the Cr–Cu ($\Delta H_{Cr-Cu} = +12$ kJ/mol) and Cr–Zr ($\Delta H_{Cr-Zr} = -12$ kJ/mol).[16] Moreover, the amount of Co addition is much more than Cr addition, leading to more pronounced chemical fluctuations. Theses two factors may result in the possibility for the occurrence of phase separation in the Cu–Zr–Al–Co alloy system is greater than that in Cu–Zr–Al–Cr alloy system. Recently, Park *et al.*[17] found atomic-scale chemical/structural fluctuations exist in the $Zr_{50}Cu_{25}Co_{12.5}Al_{12.5}$ BMG through liquid phase separation. But in the present work, nanoscale phase separation with the formation of Cu-rich and Co-rich glassy phases was detected in the alloy when the Co content is only 2 at%. The difference in the characteristic length scale for phase separation is originated from the difference in the alloy composition. In the Cu–Zr–Al–Co alloy system, the microstructure sensitively changes with the Co concentration. Compared with Cu–Zr–Al base alloy, addition of 2 at% Co in the Cu–Zr–Al–Co alloy moves the alloy composition toward the metastable miscibility gap region. The large difference heat of mixing and the moderate cooling rate associated with copper mold casting provide sufficient chemical driving force and enough time for phase separation to occur during solidification, respectively. When

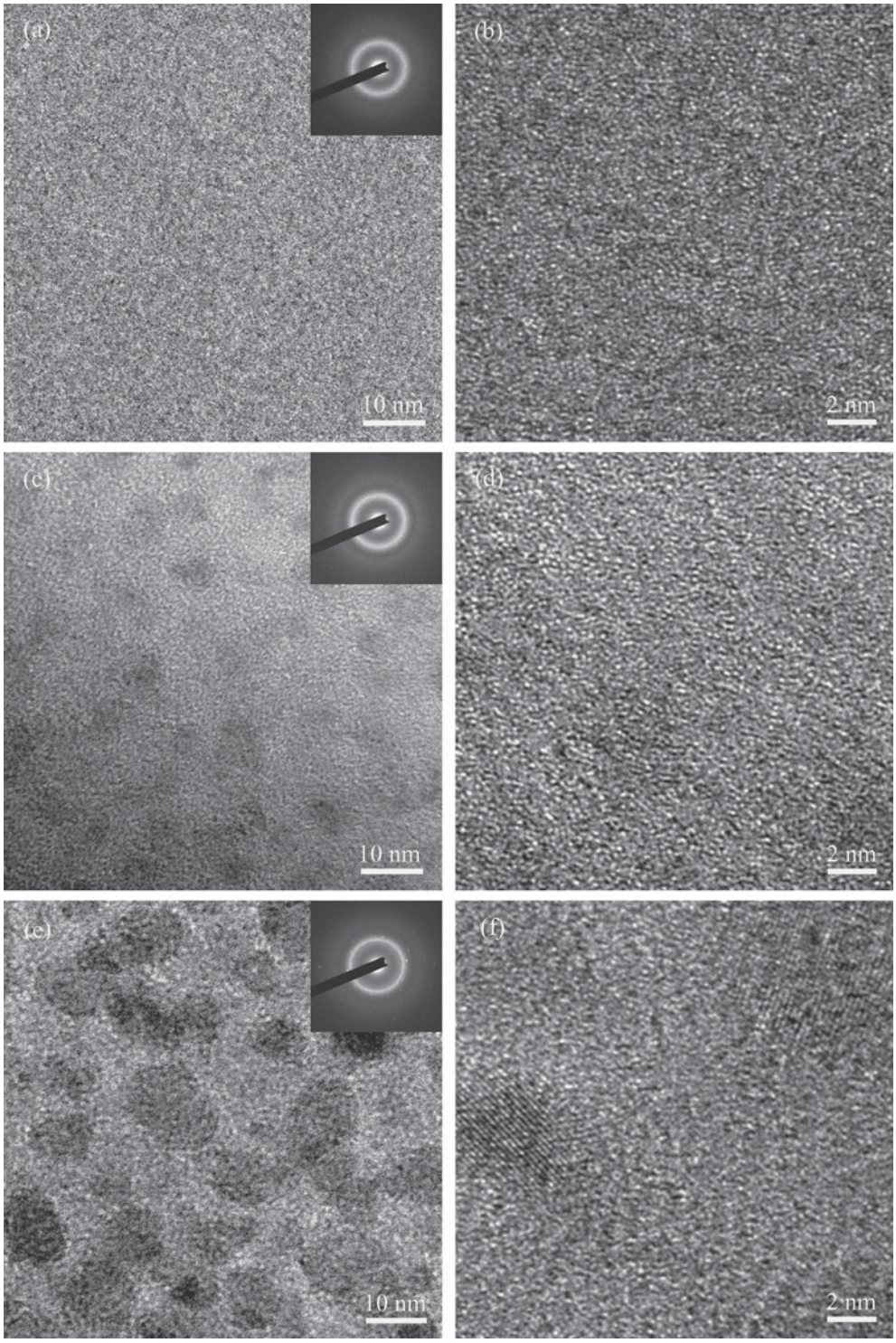

Fig. 3 TEM bright-field images, SAED patterns, and the corresponding HRTEM images for the $Cu_{46}Zr_{46}Al_8$ (a), (b), $(Cu_{46}Zr_{46}Al_8)_{98}Co_2$ (c), (d) and $(Cu_{46}Zr_{46}Al_8)_{97}Co_3$ (e), (f) rods.

the homogeneous melt is cooled below the temperature corresponding to the miscibility gap, phase separation occurs by the mechanism of nucleation and growth, and the melt would solidify into two glassy phases with different chemical compositions. With further increasing the amount of Co, more pronounced chemical fluctuations induce larger characteristic length scale for the separated liquid phase, but it could then solidify into the nanocrystalline phase due to the less glass-forming ability, and the length scale of chemical fluctuation determines the size of the nanocrytals. The present results indicate that the amorphous/amorphous or amorphous/crystalline composite structure can be selected in the $(Cu_{46}Zr_{46}Al_8)_{100-x}Co_x$ alloys by controlling the Co concentration.

The change in microstructure is expected to lead to a change in mechanical behavior as well. Figure 4 and Table 1 present the compression test results for the rod samples performed under room temperature. All the samples exhibit a

large elastic elongation of ~2%, and begin to yield at 1850–1980 MPa, followed by different degrees of plastic strain prior to failure. As the Co content increases from 0 to 4 at%, the fracture strength gradually increases from 1870 to 2002 MPa, while the plasticity initially increases from 0.04 to 1.7% at $x = 2$, and then decreases to 1.1% at $x = 4$. The typical morphologies of the external surface and the fracture surface are displayed in Fig. 5. The fracture of each sample occurs along the maximum shear stress plane, which is inclined by about 45° with respect to the compression axis. For the base alloy without Co addition, only a few shear bands can be observed on the external surface. However, intersected multiple shear bands were found for the alloy with $x = 2$. The extent of plastic deformation for BMGs depends strongly on the number of shear bands generated during deformation.[18] A high density of shear bands accounts for an enhanced plasticity, which is in accord with the stress–strain curves. The fracture surface of the base alloy exhibits a uniform vein-like pattern within the bands, which is attributed to local viscous flow during shear deformation.[19] For the alloy with $x = 2$, however, the fracture morphology reveals a mixture of vein-like pattern and intermittent smooth regions. The formation of smooth regions on the fracture surface may be closely linked with the existence of local structural heterogeneity (e.g., phase separation).[20] These smooth regions were formed during the rapid propagation of cracks when the crack tip recovered from overcoming a trap of high density local atomic packing of the glassy phase (e.g., dark glassy phase).

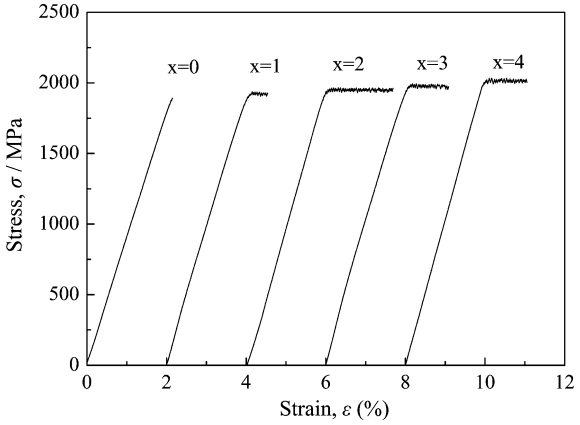

Fig. 4 Compressive stress–strain curves for the $(Cu_{46}Zr_{46}Al_8)_{100-x}Co_x$ rods.

Table 1 Measurement results of yield stress σ_y, fracture stress σ_f, yield strain ε_y and plastic strain ε_p for the $(Cu_{46}Zr_{46}Al_8)_{100-x}Co_x$ alloys.

x (at% Co)	σ_y/MPa	σ_f/MPa	ε_y/%	ε_p/%
0	1848 ± 41	1870 ± 24	2.02 ± 0.06	0.04 ± 0.02
1	1873 ± 43	1926 ± 49	1.99 ± 0.04	0.53 ± 0.15
2	1908 ± 24	1951 ± 38	2.02 ± 0.03	1.74 ± 0.36
3	1946 ± 36	1974 ± 47	2.01 ± 0.02	0.82 ± 0.27
4	1980 ± 29	2002 ± 52	2.06 ± 0.03	1.1 ± 0.34

$Cu_{46}Zr_{46}Al_8$ BMG exhibits uniform amorphous structure, and its plastic deformation at room temperature is mostly concentrated in the main shear band, resulting in rapid propagation of shear band and premature fracture. However, in the case of $(Cu_{46}Zr_{46}Al_8)_{98}Co_2$ alloy, Co has a positive heat of mixing with Cu but attractive interactions with Zr and Al, the minor addition of Co changes the atomic configuration

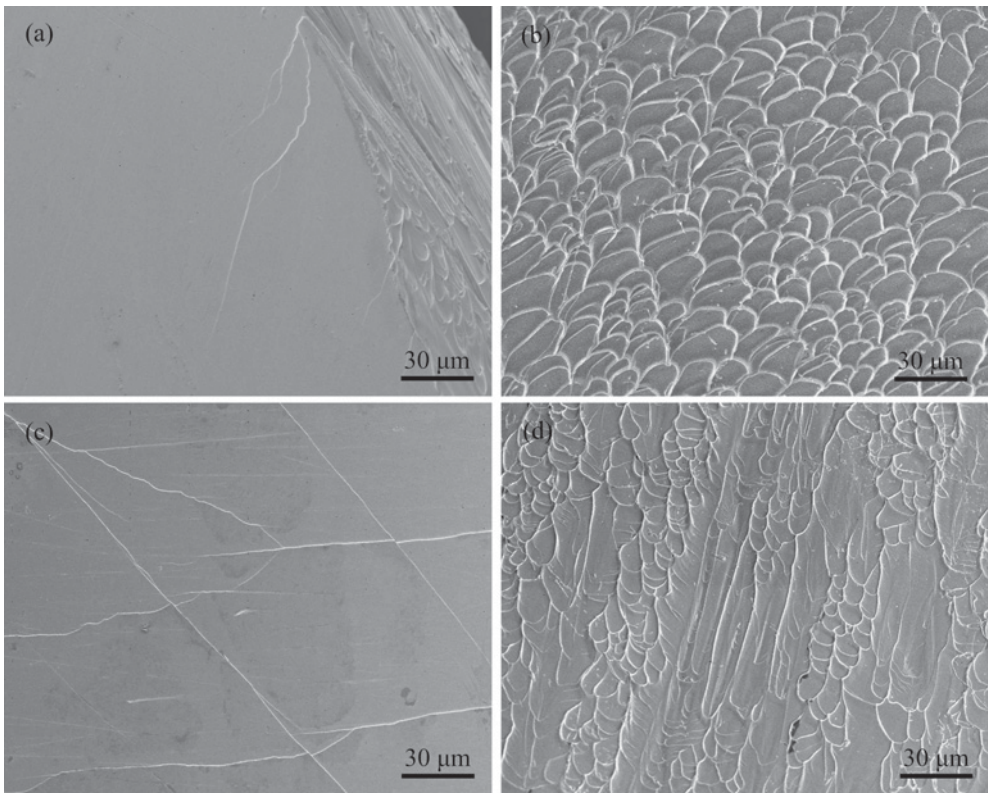

Fig. 5 SEM images of the outer appearance and fracture surface for the $Cu_{46}Zr_{46}Al_8$ (a), (b) and $(Cu_{46}Zr_{46}Al_8)_{98}Co_2$ (c), (d) rods.

and induces inhomogeneous structure with two different chemical compositions and different coordinate numbers, leading to different local critical shear stresses (CSSs) for activation of shear bands. Therefore the heterogeneous structure of the Cu–Zr–Al–Co BMG is composed of hard regions with high critical shear stress and soft regions with relatively low critical shear stress. Considering that Co–Al ($\Delta H_{\mathrm{Co-Al}} = -19$ kJ/mol) and Co–Zr ($\Delta H_{\mathrm{Co-Zr}} = -41$ kJ/mol) pairs in the Co-rich phase have stronger chemical affinity than Cu–Al ($\Delta H_{\mathrm{Cu-Al}} = -1$ kJ/mol) and Cu–Zr ($\Delta H_{\mathrm{Cu-Zr}} = -23$ kJ/mol) in the Cu-rich phase, respectively, resulting in that Co-rich phase has a higher atomic packing density than Cu-rich phase, the Cu-rich and Co-rich phases are therefore the soft and hard phases, respectively. As a result, the strengthening effect of the hard phase embedded in the matrix combined with the strong interface between the two phases leads to enhanced fracture strength for the BMG. Upon plastic deformation, shear bands are preferentially initiated in the soft Cu-rich phase, whose propagation is however impeded by the hard Co-rich phase. With further increasing the load, multiplication and branching of shear bands are activated. In other words, the heterogeneous structure acts as obstacles for the propagation of shear bands and promotes the generation of multiple shear bands, resulting in improved plasticity. For the alloy with more than 2 at% Co, an increase in the size and volume fraction of the Co-rich phase results in higher fracture strength. But the plasticity becomes worsen because of the formation of nanocrystals during cooling, which was also found in some other BMGs.[15,21,22] The present research reveals that the mechanical property can be enhanced by tailoring the phase separated microstructure properly.

4. Conclusions

(1) The microstructure of the $(Cu_{46}Zr_{46}Al_8)_{100-x}Co_x$ ($x = 0$, 1, 2, 3 and 4) alloys depends very much on the Co content. The alloy without Co addition exhibits uniform amorphous structure, while addition of an appropriate amount of Co ($x \geq 2$) moves the alloy composition toward the miscibility gap region, and phase separation takes place during cooling, forming droplet-type structure. The characteristic length scale for phase separation increases with increasing the Co content. Depending on the glass-forming ability of the separated liquid phase, amorphous/amorphous or amorphous/crystalline composite structure can be formed.

(2) The fracture strength of the BMG continuously increases with the Co content. Meanwhile, the plasticity can be improved effectively by addition of 2 at% Co, which is attributed to the occurrence of phase separation into Cu-rich and Co-rich glassy phases. But it becomes deteriorated due to nanocrystallization when the Co content is more than 2 at%. The present research reveals that development of bulk-type phase-separating glassy alloy by minor alloying addition provides a hint for the improvement of the mechanical properties of BMGs.

Acknowledgements

The authors are grateful for the financial supports of the National Natural Science Foundation of China (Grant Nos. 50831003 and 50771064), the National Basic Research Program of China (Grant No. 2011CB610405), and Shanghai Pujiang Program (Grant No. 10PJ1405900).

REFERENCES

1) D. C. Hofmann, J. Y. Suh, A. Wiest, G. Duan, M. L. Lind, M. D. Demetriou and W. L. Johnson: Nature **451** (2008) 1085–1089.
2) H. Bei, S. Xie and E. P. George: Phys. Rev. Lett. **96** (2006) 105503.
3) J. M. Liu, X. G. Yuan, H. F. Zhang, H. M. Fu and Z. Q. Hu: Mater. Trans. **51** (2010) 1033–1037.
4) F. X. Qin, X. M. Wang and A. Inoue: Mater. Trans. **48** (2007) 2390–2394.
5) H. Choi-Yim, R. D. Conner, F. Szuecs and W. L. Johnson: Acta Mater. **50** (2002) 2737–2745.
6) L. Liu, C. L. Qiu, H. Zou and K. C. Chan: J. Alloy. Compd. **399** (2005) 144–148.
7) Y. H. Liu, G. Wang, R. J. Wang, D. Q. Zhao, M. X. Pan and W. H. Wang: Science **315** (2007) 1385–1388.
8) L. Y. Chen, Z. D. Fu, G. Q. Zhang, X. P. Hao, Q. K. Jiang, X. D. Wang, Q. P. Cao, H. Franz, Y. G. Liu, H. S. Xie, S. L. Zhang, B. Y. Wang, Y. W. Zeng and J. Z. Jiang: Phys. Rev. Lett. **100** (2008) 075501.
9) J. C. Oh, T. Ohkubo, Y. C. Kim, E. Fleury and K. Hono: Scr. Mater. **53** (2005) 165–169.
10) X. H. Du, J. C. Huang, K. C. Hsieh, Y. H. Lai, H. M. Chen, J. S. C. Jang and P. K. Liaw: Appl. Phys. Lett. **91** (2007) 131901.
11) D. H. Pi, J. K. Lee, M. H. Lee, S. Yi, J. Eckert and K. B. Kim: J. Alloy. Compd. **486** (2009) 233–236.
12) E. S. Park and D. H. Kim: Acta Mater. **54** (2006) 2597–2604.
13) Q. S. Zhang, W. Zhang, G. Q. Xie and A. Inoue: Mater. Sci. Eng. B **148** (2008) 97–100.
14) K. B. Kim, J. Das, F. Baier, M. B. Tang, W. H. Wang and J. Eckert: Appl. Phys. Lett. **88** (2006) 051911.
15) W. Zhou, L. T. Kong, J. F. Li and Y. H. Zhou: J. Mater. Sci. **47** (2012) 4996–5001.
16) A. Takeuchi and A. Inoue: Mater. Trans. **46** (2005) 2817–2829.
17) J. M. Park, J. H. Han, N. Mattern, D. H. Kim and J. Eckert: Metall. Mater. Trans. A **43** (2012) 2598–2603.
18) Z. F. Zhang, J. Eckert and L. Schultz: Acta Mater. **51** (2003) 1167–1179.
19) J. Eckert, J. Das, S. Pauly and C. Duhamel: J. Mater. Res. **22** (2007) 285–301.
20) E. S. Park, H. J. Chang, J. S. Kyeong and D. H. Kim: J. Mater. Res. **23** (2008) 1995–2002.
21) K. Mondal, T. Ohkubo, T. Toyama, Y. Nagai, M. Hasegawa and K. Hono: Acta Mater. **56** (2008) 5329–5339.
22) L. Q. Xing, C. Bertrand, P. P. Dallas and M. Cornet: Mater. Sci. Eng. A **241** (1998) 216–225.